RESEARCH ARTICLE

# Early spectral dynamics are indicative of distinct growth patterns in post-wildfire forests

Sarah Smith-Tripp[1] (iD), Nicholas C. Coops[1], Christopher Mulverhill[1], Joanne C. White[2] (iD) & Sarah Gergel[3]

[1]Department of Forest Resources Management, Forest Sciences Center, University of British Columbia, 2024-2424 Main Mall, Vancouver V6T 1Z4, British Columbia, Canada
[2]Canadian Forest Service (Pacific Forestry Centre) Natural Resources Canada, 506, West Burnside Road, Victoria V8Z 1M5,British Columbia, Canada
[3]Department of Forest and Conservation Sciences, Forest Sciences Center, University of British Columbia, 3024-2424 Main Mall, Vancouver V6T 1Z4,British Columbia, Canada

doi: 10.1002/rse2.420

## Abstract

Western North America has seen a recent dramatic increase in large and often high-severity wildfires. After forest fire, understanding patterns of structural recovery is important, as recovery patterns impact critical ecosystem services. Continuous forest monitoring provided by satellite observations is particularly beneficial to capture the pivotal post-fire period when forest recovery begins. However, it is challenging to optimize optical satellite imagery to both interpolate current and extrapolate future forest structure and composition. We identified a need to understand how early spectral dynamics (5 years post-fire) inform patterns of structural recovery after fire disturbance. To create these structural patterns, we collected metrics of forest structure using high-density Remotely Piloted Aircraft (RPAS) lidar (light detection and ranging). We employed a space-for-time substitution in the highly fire-disturbed forests of interior British Columbia. In this region, we collected RPAS lidar and corresponding field plot data 5-, 8-, 11-,12-, and 16-years postfire to predict structural attributes relevant to management, including the percent bare ground, the proportion of coniferous trees, stem density, and basal area. We compared forest structural attributes with unique early spectral responses, or trajectories, derived from Landsat time series data 5 years after fire. A total of eight unique spectral recovery trajectories were identified from spectral responses of seven vegetation indices (NBR, NDMI, NDVI, TCA, TCB, TCG, and TCW) that described five distinct patterns of structural recovery captured with RPAS lidar. Two structural patterns covered more than 80% of the study area. Both patterns had strong coniferous regrowth, but one had a higher basal area with more bare ground and the other pattern had a high stem density, but a low basal area and a higher deciduous proportion. Our approach highlights the ability to use early spectral responses to capture unique spectral trajectories and their associated distinct structural recovery patterns.

# Introduction

Monitoring forest recovery in response to changing fire regimes is a global challenge accentuated in western North America, where a warmer climate has recently dramatically increased wildfire occurrence (Parisien et al., 2023). Pervasive wildfires and subsequent recovery of forests in a warmer climate may change forest structure by altering stand density (Hoecker et al., 2023), shifting dominance of coniferous tree species (Jorgensen et al., 2023), or even triggering ecosystem transitions such as forest to grassland (Hamilton & Burton, 2023). Such novel patterns of recovery have already been observed in the boreal, where increased fire frequency and intensity has led to increases in postfire deciduous cover (Baltzer et al., 2021; Johnstone et al., 2010). To characterize these possibly novel recovery patterns, forest managers require spatially and temporally continuous assessments of regeneration early in the recovery period (first 5–10 years), as this early period defines long-term forest structure (Seidl & Turner, 2022).

Observations from satellites, aerial imagery, and light detection and ranging (lidar) allow postfire recovery assessment across broad, compositionally diverse landscapes (White, 2024). Optical satellite imagery is especially applicable for recovery monitoring due to the availability of a long and dense time series (Pasquarella et al., 2016; White et al., 2020). Using satellite image archives, such as those of Landsat, changes in spectral reflectance over time can be associated with forest recovery (Kennedy et al., 2012). Spectral trajectories are related to, but are not a direct measure of forest structure (Chu & Guo, 2014; Cohen et al., 2010; Kiel & Turner, 2022; White et al., 2022). However, when fused with field or other structural data, spectral reflectance can help characterize structural attributes indicative of recovery (White et al., 2023). Some key indicators for structural recovery patterns (henceforth recovery patterns) include measures of stand structure and composition such as stem density, composition, basal area (BA), and biomass (Johnstone et al., 2016). Prior work has linked spectral observations to these structural attributes (Kemp et al., 2016; Kiel & Turner, 2022; White et al., 2019, 2020). More recently, White et al. (2023) used a North American boreal-wide set of field data to show that areas of boreal forest with faster spectral recovery were also more likely to have transitioned from a coniferous forest prefire to a deciduous forest postfire, or were deciduous prefire. However, research of distinct structural recovery patterns is often retrospective, identifying novel patterns after stand establishment (Davis et al., 2023).

To address widespread calls to manage forests to maintain carbon storage (Clason et al., 2022; Metsaranta et al., 2023), mitigate future fire risk (Hessburg et al., 2021), and ensure future timber supplies (North et al., 2019), new techniques are needed to identify spatially variable recovery patterns within the time window that defines the onset of forest recovery (henceforth, recovery onset, which can be as short as 5 years; Frazier et al., 2018). One approach to capture recovery onset is to substitute space-for-time, using similar sites at different stages of postfire recovery and projecting how a site at an earlier stage may develop to a site at a later stage (Pickett, 1989). Site similarities can be derived from optical satellite imagery. For example, Ye et al. (2021) use Landsat data to show that distinct decreases in spectral reflectance were linked to the likelihood and severity of future insect disturbance. The same logic suggests that areas with similar spectral responses at the onset of recovery may also have similar patterns of structural recovery.

Linking spectral trajectories to temporal patterns of structural recovery relies on field campaigns to gather measures of key recovery indicators. In postfire environments, relying on field campaigns to relate to satellite-based spectral observations requires personnel to work in remote and potentially dangerous areas (Rakochy & Hawkins, 2006). Further, resource demand for field sampling campaigns increases when more samples are needed to capture diverse spectral or structural responses of extensive burns in diverse forest types (Bartels et al., 2016; Holsinger et al., 2022). Thus, field sampling may be unrealistic to capture the diverse structural responses of increasingly fire-prone North American forests. One resource to augment structural data gathered with intensive field methods are data from remotely piloted aircrafts (RPAS), which can come equipped with low-cost lidar systems (Coops et al., 2021). RPAS-acquired lidar can extend assessment of forest stand characteristics to remote and/or challenging locations at low costs (Guimarães et al., 2020; Wulder et al., 2013) while maintaining or even improving accurate measures of the fine-scale vegetation characteristics that define young and regenerating forests (Shrestha et al., 2021). Using spatially continuous estimates of forest structure from RPAS, measures of structural recovery can be linked to distinct spectral trajectories (Smith-Tripp et al., 2024). However, it remains to be investigated whether distinct spectral trajectories identified early on (i.e., 5 years after a disturbance) are indicative of later structural recovery patterns.

In this study, we asked whether Landsat spectral trajectories identified 5 years after a wildfire event are indicative of different patterns of structural forest recovery. Overall, this study had two main objectives. First, we identified unique spectral responses from Landsat metrics derived 5 years after the fire event (within the recovery onset period). Second, we grouped these spectral trajectories based on patterns in structural recovery identified from a space-

for-time substitution in forests 5–16 years after fire. Using RPAS, we acquired structural measures prioritized by forest managers, including stem counts, BA, composition, and the proportion of bare ground. We used space-for-time RPAS data to describe temporal patterns of recovery and group spectral trajectories that behave with distinct patterns. By grouping spectral trajectories, we aimed to investigate distinct patterns of structural recovery in burned landscapes of the interior of British Columbia.

# Materials and Methods

## Study area

Our work focused on an area in central British Columbia, Canada, which is representative of other ecosystems in western North America. The area spans over 12 million ha of sub-boreal spruce (SBS) and sub-boreal pine spruce (SBPS) ecozones of interior British Columbia (Fig. 1). The SBS and SBPS bio-geoclimatic ecozones (BEC) are prone to large and high-severity wildfires with return intervals greater than 100 years (Meidinger & Pojar, 1991). These forests are dominated by lodgepole pine (*Pinus contorta*), interior spruce (*Picea glauca*), sub-alpine fir (*Abies lasiocarpa*), and trembling aspen (*Populous tremuloides*), which are similar to other dry continental forests in North America and thus have broad applications to operationalizing methods to monitor structural forest recovery (Klassen & Burton, 2015).

Fire-disturbed areas, including both year and severity, were provided by the National Terrestrial Ecosystem Monitoring System (Hermosilla et al., 2018). NTEMS supplied fire severity as a measure of dNBR (difference in the Normalized Burn Ratio – the ratio of red and the short-wave spectral bands before and after disturbance). To identify high-severity areas, we selected pixels where dNBR values ranged from 1.5 standard deviations below the mean to the maximum dNBR value for all pixels designated as high severity per the provincial classification (BC Ministry of Forests, 2021). We also omitted areas that had been replanted after the fire. Locations of high-severity fire, where final spectral clustering was applied, covered 657 000 hectares (5.4%) of the study area from 1984 to 2018.

## Data processing

### Spectral metrics from Landsat satellite imagery

#### Landsat best-available pixel composites

The temporal spectral metrics used to develop the unique spectral trajectories were created from time series of Landsat observations. Time series of Landsat spectral observations were derived from cloud-free image composites developed using a Best Available Pixel (White et al., 2014) compositing approach. BAP images were downloaded from Google Earth Engine for 1984–2022 (Francini, 2021). Selected pixels prioritized images closest to August 1st (corresponding to the peak of the growing season for Canadian forests) with minimal cloud cover (White et al., 2014). We excluded pixels more than 30 days from August 1st or Landsat scenes that had more than 70% cloud cover. We additionally applied a despiking algorithm with a tolerance of 0.7, which uses surrounding year values to fill pixels where the difference from the prior year is large (>70% change) and also not observed in later years (Hermosilla et al., 2024). We selected this higher value (often set at 0.2 or lower) to capture disturbances without marking them as noise (Cohen et al., 2010).

### Spectral trajectory variables

We derived Landsat indices known to differentiate forest attributes (Frolking et al., 2009). Indices included the Normalized Burn Ratio (NBR), Normalized Difference Vegetation Index (NDVI), Normalized Difference Moisture Index (NDMI), and the tasseled cap transformations —greenness (TCG), wetness (TCW), brightness (TCB), and angle (TCA). We calculated spectral metrics based on a 5-year window after the fire disturbance. Using this 5-year window, three metrics that described variability in postfire spectral response were calculated for each fire-disturbed pixel. Spectral metrics included the magnitude of regrowth between the minimum postdisturbance value and the value 5 years later ("regrowth magnitude"), the median rate of change after the fire (theil-sen slope or "slope"), and the index measure 5 years after the fire (index +5 years; see Fig. 2). We also included the magnitude of the disturbance ("dist mag") for a total of 22 variables that described trajectories of the seven selected spectral indices. To calculate spectral variables, pixels had to have more than three postdisturbance cloud-free images within 5 years after fire.

### Space-for-time forest structure data with RPAS lidar

To understand temporal patterns in structural recovery, we built a space-for-time structural dataset of RPAS lidar data collected in forests 5–16 years after forest fire. In total, we acquired 1380 hectares of lidar data with an average point density of 374 points/m$^2$ (Fig. 1). We normalized the lidar data by progressively filtering points to create a digital elevation model that we subtracted from above-ground points to normalize canopy height (Klápště et al., 2020). We
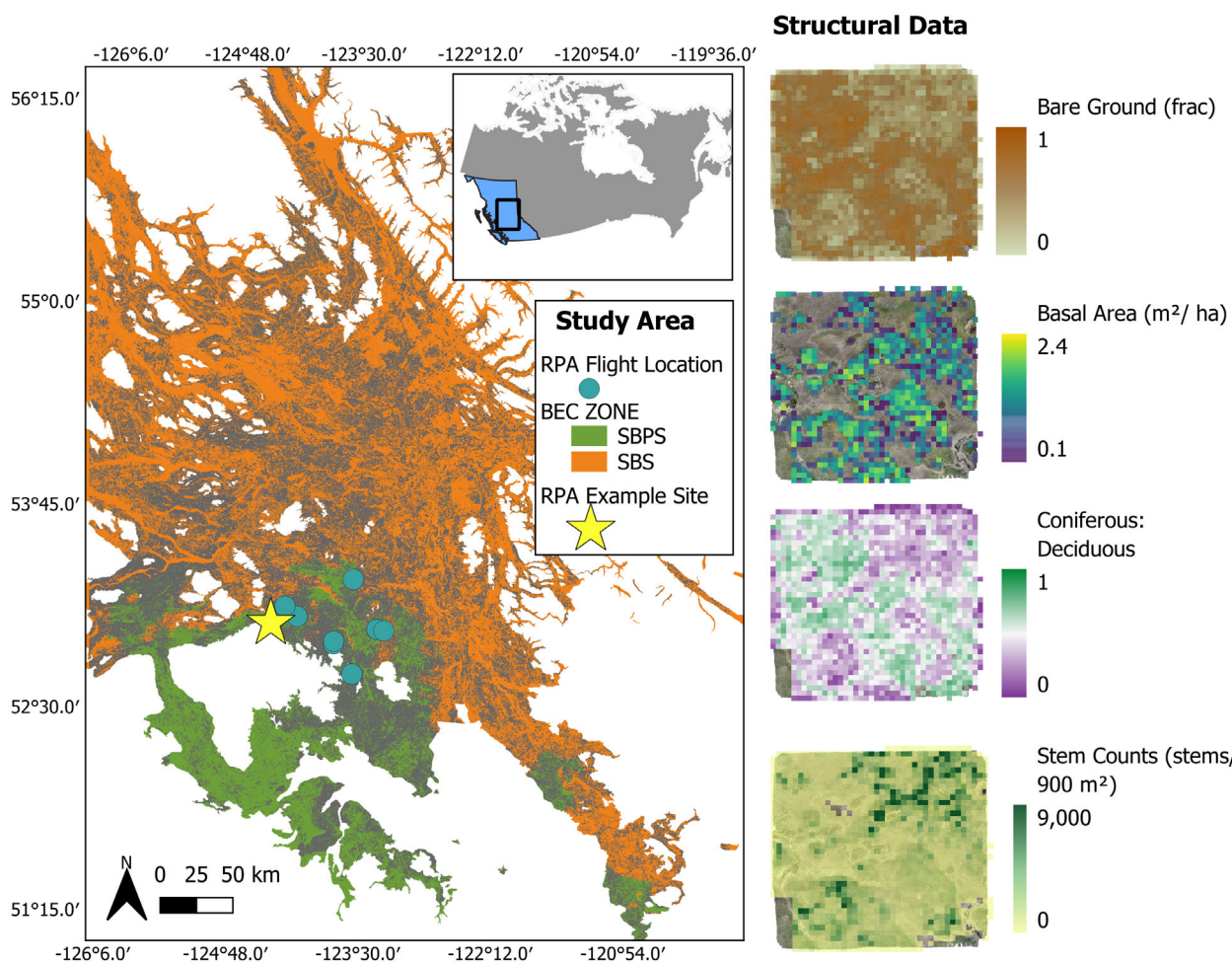
**Figure 1.** (Left) Location of BEC Zones included in the study (SBS: Sub-Boreal Spruce, SBPS: Sub-Boreal Pine Spruce). Areas covered in gray were disturbed 1984–2022. Blue dots represent Lidar flight locations. The inset map shows the location of British Columbia and the study site (black box) in Canada. The yellow star notes the location selected as an example for lidar data at right. (Right) Examples of the lidar variables include proportion of bare ground, basal area, coniferous to deciduous ratio, and stem counts.

computed standard metrics (Roussel et al., 2020) to use as inputs for generalized linear models (GLMs) applied to validation data from 26 field plots collected in the same year of lidar acquisition. Final selected forest structural predictions included: bare ground (%), basal area (BA, m²/ha), the ratio of coniferous to deciduous (coniferous: deciduous), and stem counts (stems/Landsat pixel). For more details on data processing and structural model development, see Smith-Tripp et al. (2024).

## Methods

To understand the different patterns of forest recovery, we combined unique satellite spectral trajectories with distinct patterns of forest structure. Structural measures from RPAS data captured multiple years postfire (5, 8, 12, and 16 years), in order to describe structural development over time. Reflecting the study objectives, our methodological approach was divided into two parts: (1) unique spectral cluster development and (2) relation of the spectral clusters with distinct structural patterns identified from the spatiotemporal structural data from RPAS. For the first objective, we used K-means clustering to identify unique spectral trajectories within high burn severity areas. For the second objective, we related these clusters of unique spectral trajectories with distinct forest structural characteristics identified using space-for-time sampling of the lidar data. We also describe the spatial distribution of these distinct patterns of forest structure. An overview of the workflow is described in Figure 2.
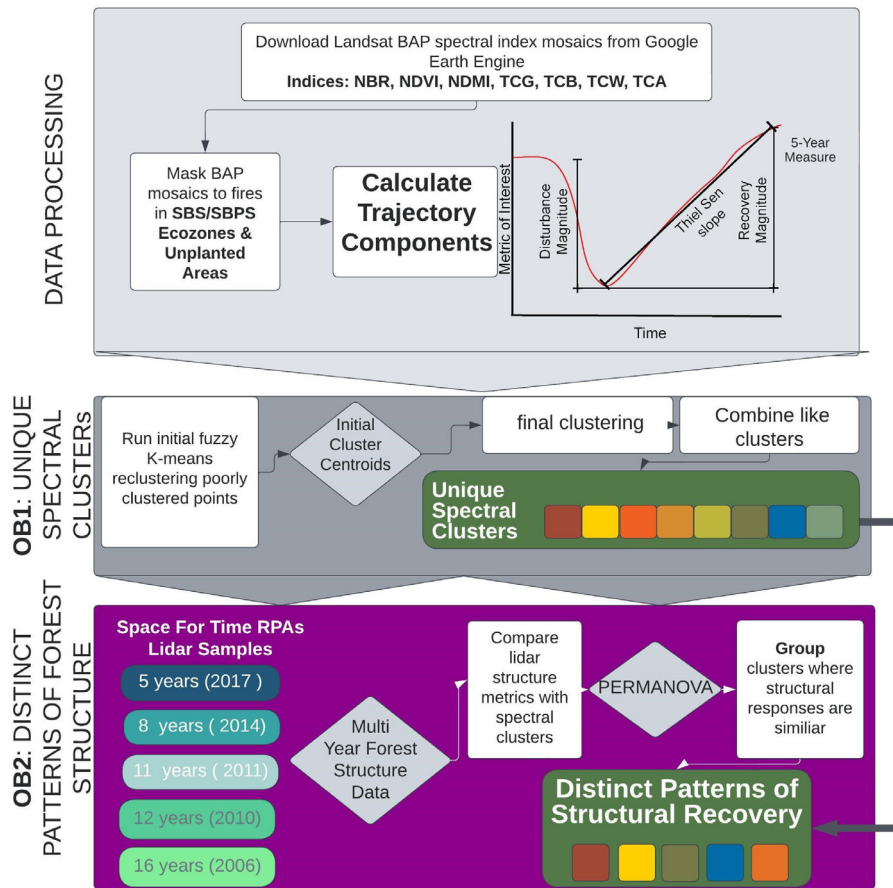
**Figure 2.** Description of landsat data processing, spectral clustering, and spatiotemporal analyses with RPAs lidar data.

## Objective 1: identifying unique spectral clusters

Spectral clusters were generated using the 22 trajectory variables (Fig. 2). Clustering used an augmented two-step k-means++ clustering algorithm, where the k-means algorithm uses informed seeds to select the (a) optimal cluster number and (b) approximate cluster centroids (Kapoor & Singhal, 2017). In this algorithm, initial cluster centers were identified using the distortion criterion, which minimizes the distance between observations and the associated cluster centroid (Kodinariya & Makwana, 2013). Using initial centroids, we applied a fuzzy k-means clustering to calculate the probability surface of each centroid (Sanderson & Curtin, 2016). For points where cluster likelihoods were less than 0.7, we ran additional clustering to identify the ideal number and approximate location of additional centroids. Centroids from both clusters seeded the final clustering matrix. From the final clustering matrix, we calculated the similarity of centroids, where centroids with shared similarities, based on the distortion criterion, were combined to produce clusters that together

describe unique spectral trajectories. We used a principal component analysis (PCA) to explore underlying variability in spectral variables used to cluster. PCA loadings described the variability that resulted in final clustering. To understand the temporal dynamics of spectral recovery, we also investigated the measures of recovery compared to predisturbance values for years 0–20. This twenty-year time period was chosen to capture the longer-term patterns of spectral recovery.

## Objective 2: characterizing distinct patterns of structural recovery

Distinct structural recovery patterns were created by combining RPAS lidar data with spectral clusters. Specifically, we combined spectral clusters where RPAS lidar supported similar structural patterns among sample years (5, 8, 11, 12, and 16 years). For example, two spectral clusters would collapse if they had significantly different stem counts but similar basal areas across sample years. To determine structural similarities, we used a permutation

multivariate analysis of variance (PERMANOVA) and posthoc pairwise comparison (Anderson, 2001). A PERMANOVA measures the significance of the distance between groups in n-dimensional space, where n is equal to the number of structural metrics ($n = 4$, the four modeled structural attributes). Significant ($P < 0.05$) PERMANOVA results supported structural differences among spectral clusters. The PERMANOVA was built on a Euclidean distance matrix of the four structural metrics. We used the distance matrix to run a PERMANOVA with 999 permutations using the distance matrix of structural measures with year treated as a factor (Anderson, 2001). Posthoc comparisons, using a Wilks test for nonparametric data, then identified which clusters could be combined based on structural similarities. We tested merged structural patterns for differences in estimates of specific structural measures, like BA, with a nested ANOVA. Nested ANOVAs were fit using year as a factor; thus, comparisons were limited to the structural patterns that had observations for all years. Final outputs of the PERMANOVA and posthoc tests identified distinct structural recovery patterns. For the ease of the reader, we gave these patterns ecologically relevant names that describe their structural patterns.

### Software packages

Clustering of spectral metrics was performed in R (R Core Team, 2023) using the *ClusterR* package (Mouselimis, 2023) for clustering, the *fpc* package (Cohen et al., 2003) to assess cluster similarity, and the *factoextra* to calculate PCA loadings (Kassambara & Mundt, 2016). Later, distinct structural types were calculated in R (R Core Team) using the *vegan* package (Oksanen et al., 2022) with posthoc tests run using the *RVAideMemoire* package (Herve, 2023). Posthoc tests of a nested ANOVA used the *rstatix* package (Kassambara & Mundt, 2016).

## Results

### Objective 1: unique spectral clusters

#### Spectral cluster prevalence

K-means clustering and combination of similar clusters resulted in 8 unique spectral clusters that explained 52% of the variance in spectral metrics. Dominant determinants of variance in clustering were the trajectory metrics for TCA and NBR (loading magnitudes for NBR regrowth = 0.25 and NBR slope = 0.27, Fig. 3B). Cluster 5 had the greatest average distance from other cluster centers (0.91), while cluster 3 had the smallest distance to other clusters (0.84; Fig. 3). Cluster 1 was the most frequently observed cluster (37% of the landscape), followed by cluster 3 (16% of the landscape). Cluster 2 was the least frequently observed (1% of the landscape).

### Spectral trajectories of clusters

Postfire clusters were derived from spectral metrics at 5 years, but clusters showed variability in spectral recovery throughout the early recovery time period (+20 years, Fig. 4). Across all clusters, indices dropped immediately postfire and slowly recovered, with many clusters recovering to prefire values within 20 years. Conversely, TCB increased for most clusters after fire. Of the indices that decreased, TCG was the first to recover to predisturbance values.

Overall rates of recovery differed among clusters and indices. Of the clusters, cluster 3 had the highest average recovery for the first 5 years after fire for all indices except NDMI and TCA. Cluster 5 had the lowest slopes for all indices except NDMI and TCA (Figure S3). For cluster 6, the onset of recovery generally occurred later (Fig. 4) compared to the other clusters. This pattern is most apparent in NBR, NDMI, and TCA.

## Objective 2: characterizing distinct patterns of structural recovery

### Structural data for each spectral cluster

RPAS lidar data covered 722 ha of spectrally clustered area (0.12% of area included in spectral clustering). The greatest overlap with space-for-time lidar samples was in areas 5 years postfire (40.1%), coinciding with areas that burned in 2017 (Fig. 5). Areas 8- and 16-years postfire were the second and third most commonly captured (23.2% and 21.3%, respectively). Of spectral clusters, cluster 1 had the largest area with RPAS structural data (304 ha). Cluster 2 had a very low proportion of area covered (~1 ha or 25 pixels). Our results focus on clusters where the number of structural samples within and across years was consistent (i.e., 1, 3, 5, 7, and 8). In clusters where the number of structural samples was low within and across years, we treat differences in structural estimates with caution.

### Spectral clusters demonstrate forest succession with distinct trends

Patterns of structural development were variable among the different structural metrics we investigated. Results of a pairwise PERMANOVA supported differences in structural metrics over time among clusters ($F_{(7, 7882)} = 173.91$, $P < 0.001$, Table S3). Using a posthoc Wilks' test, we found spectral clusters 3, 4, 5, and 8 had similar structural patterns both within and across years ($P > 0.05$, Figure S3). Therefore, these clusters were combined under one
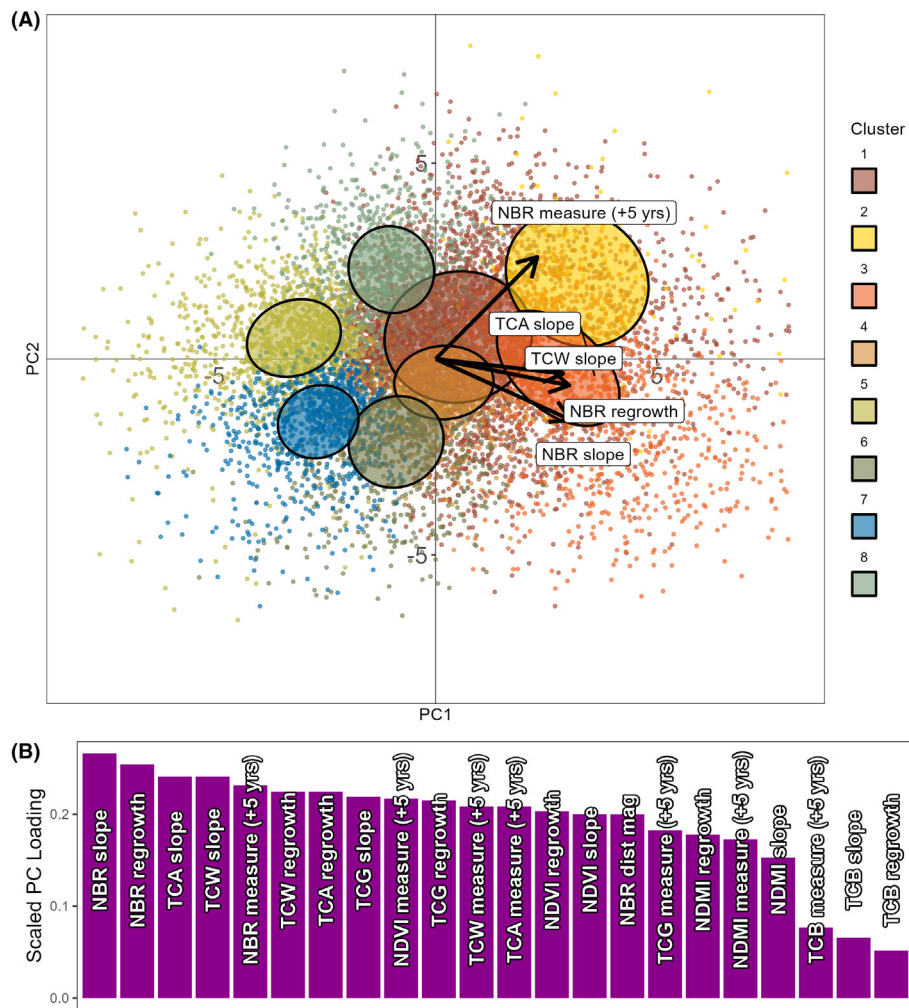
**Figure 3.** (A) Principal component analysis of trajectory variables used in clustering. Points represent a sample of the total dataset (10 000 random samples weighted by cluster frequency). Ellipses define where 40% of the data for each cluster are included. Black-labeled arrows are the variable loadings of the PCA. Colors denote associated spectral cluster. (B) Variable loadings in order of importance. Values are scaled relative to the importance of each principal component.

structural label. For simplicity, we assign ecologically relevant names to structural patterns based on observed structural dynamics in response data. These were:

- **Emergent conifer**: representing cluster 1. This pattern showed a strong deciduous response (71% deciduous in year 5) in early years that was replaced by relatively large coniferous stems (BA 0.47 m$^2$/ha in year 12 and BA 0.82 m$^2$/ha in year 16)
- **Mixed forest regrowth**: representing clusters 3, 4, 5 and 8. In this group, a high number relatively small coniferous stems (553 stems/ha in year 12 and 866 stems/ha in year 16) were accompanied by a mix of woody deciduous shrubs (10% deciduous cover in year 16).

- **Residual canopy to late growth**: representing cluster 2. This class had a live canopy after the fire that senesced within the first 8 years (BA 2.14 in year 5 and BA 0.27 in year 8)
- **Stem exclusion to stem loss:** representing cluster 6. In this pattern, a high number of coniferous stems in years 8 and 12 was not observed in year 16 (820 stems/ha in year 12 and 384 stems/ha in year 16).
- **Dense mixed cover:** representing cluster 7. Generally, this pattern had high ground cover of both deciduous and coniferous (coniferous: deciduous ratio 0.89 in year 12) while the proportion of coniferous stems was temporally variable. Similar to the pattern above, this pattern also had a large number of stems in year 12.
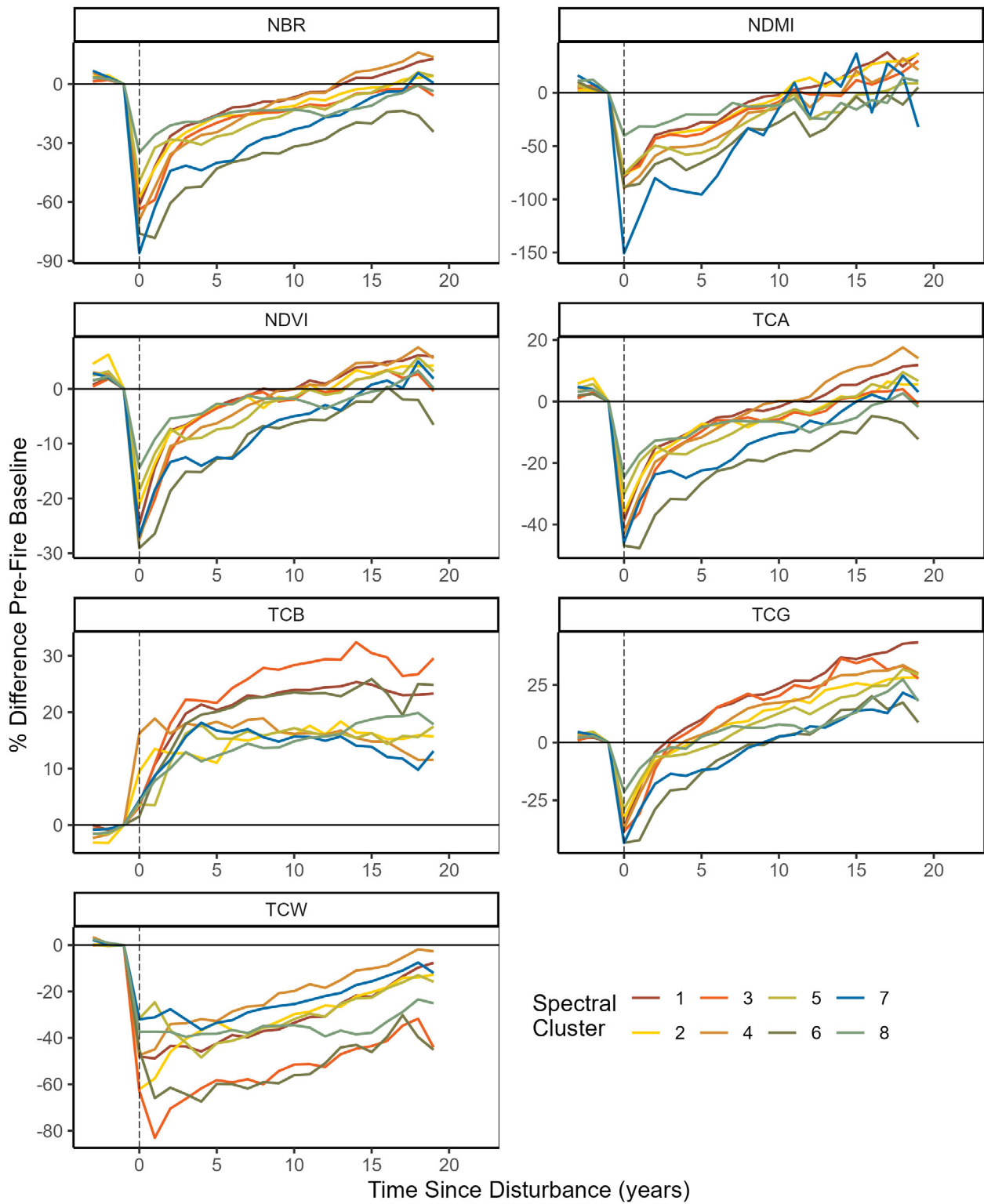
**Figure 4.** Mean trajectories for each spectral cluster for all indices for years −3 to +20 after fire. Mean values are relative to a 3-year pre-disturbance baseline period for all clusters. Label above panel notes respected index. The black dotted line at year = 0 is the fire year.
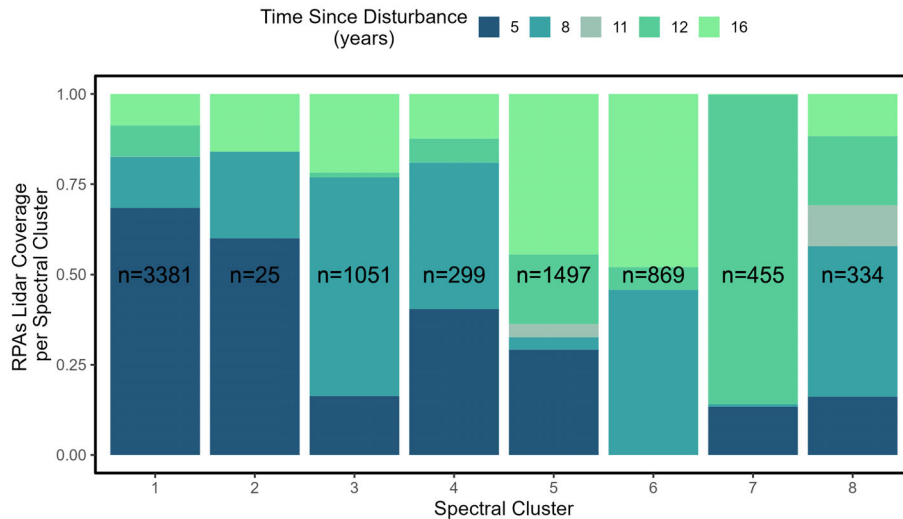
**Figure 5.** Number of pixels for each spectral cluster with associated RPA lidar data. The total value for each cluster is noted in the column. Colors denote the proportion of pixels by fire year for each cluster.

For the five named groups, we compare their temporal patterns of structural recovery for every sample year (Fig. 6). Of the structural patterns, emergent conifer and mixed forest regrowth were the only patterns that did not have years with missing data. Emergent conifers had the highest BA 16 years after the fire (0.82 ± 0.002 m²/ha (standard error), Table S4). Comparatively, the residual canopy to late growth class had the lowest BA (0.42 ± 0.15 m²/ha). Stem counts showed an inverse pattern between these two groups: 16 years after fire, low-density areas had the lowest stem count estimates (520 ± 2 stems/900 m²), and the residual canopy group had the highest stem count estimates (841 ± 128 stems/ 900 m²; Figure 6). However, the number of observations for the residual canopy group in year 16 was low (n = 4). Of the spectral groupings with more data in year 16, stem exclusion to stem loss had the highest stem count estimates (652 ± 1 stems/900 m², n = 384). Yet, the high density of stems in this group was a decrease from observations at 12 years after fire, where, for the same group, stem count estimates were 820 (±10) stems/900 m².

### Spatial distributions of distinct structural patterns

Over 80% of the study area was covered by mixed forest (45.5%) and emergent conifer (36.9%). The skewed distribution of structural patterns is highlighted in Figure 7, which shows the dominant structural group averaged over 10,000 ha hexagons. The least common pattern was residual canopy to late growth (1.18%). In most areas, all distinct structural patterns were observed (5 distinct observations per hexagon). Emergent conifers or mixed forest regrowth groups were generally the dominant structural pattern, but dense mixed cover was more common in the southern part of the landscape.

We highlighted the differences in structural development for the two most common patterns, emergent conifer and mixed forest, which both had consistent structural measures within and across years (Fig. 4). We directly compared the structural estimates of emergent conifer and mixed forests, as well as how these structural estimates varied compared to the overall distribution of the structural data for a given year. Areas identified as emergent conifer had significantly different estimates of forest structure compared to areas identified as mixed forest regrowth (Table S5). For emergent conifers, early years (5–12 years) were generally more deciduous and had a lower proportion of bare ground compared to mixed forest areas. From year 5 through 16, emergent conifers trended less deciduous than other regions (Fig. 6). By year 16, mixed regrowth had a higher proportion of deciduous and less bare ground than the emergent conifer class. In year 16, the mixed regrowth class had the highest ratio of deciduous cover (~1 m² deciduous for every 10 m² of coniferous cover), while the emergent conifer had half as many deciduous (Fig. 8). For most years, emergent conifers also had higher BA estimates compared to mixed forest regions (Fig. 8).

## Discussion

Larger and more severe wildfires across much of western North America underscore the need for efficient monitoring, capable of capturing the development of possibly
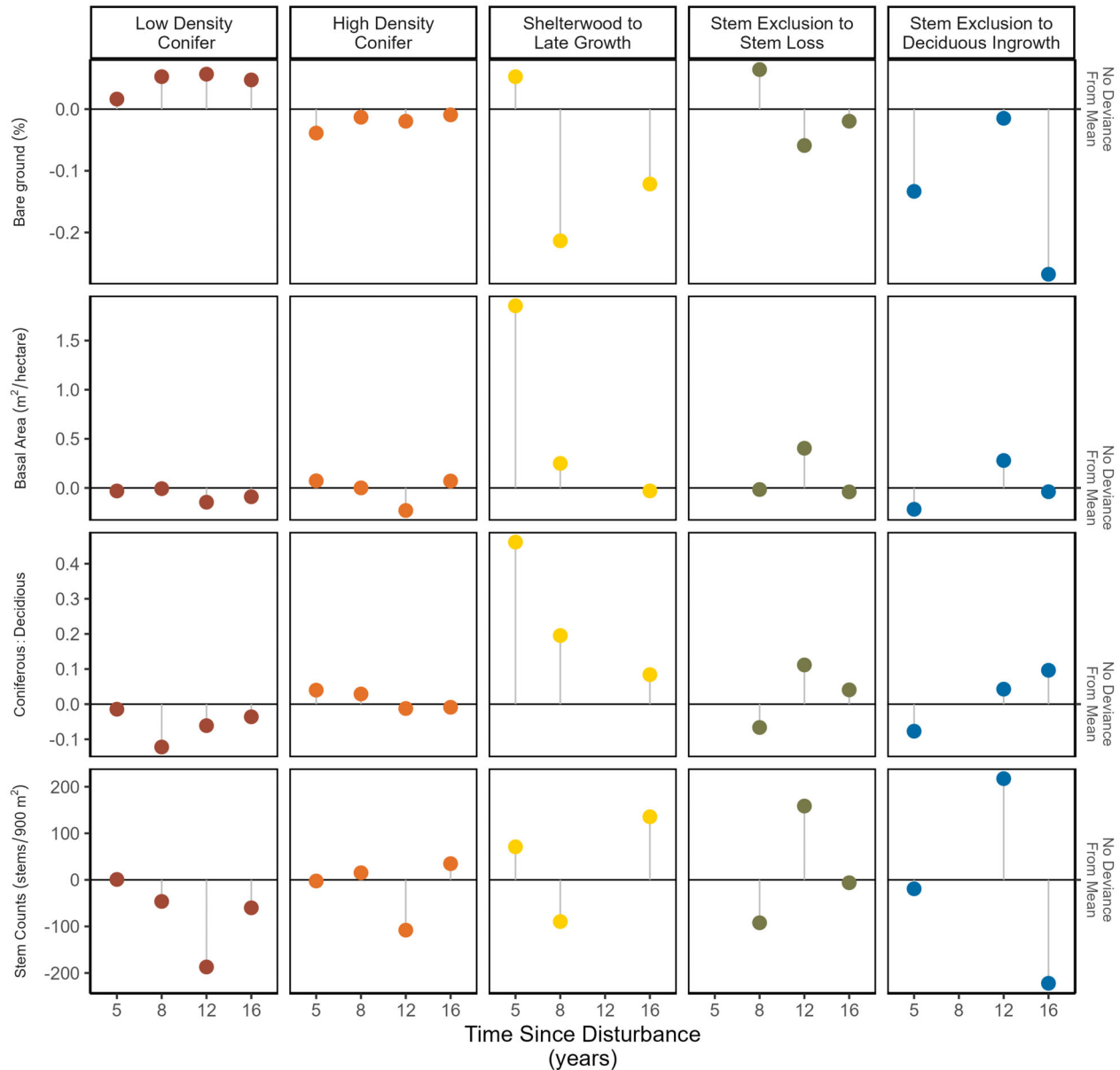
**Figure 6.** The difference between the mean for each spectral pattern and the mean for each year since fire (5, 8, 11, 12, and 16 years). The horizontal black line is the mean for that year. For bare ground percentage, values above the line have more bare ground. For coniferous: deciduous, points above the line have a higher proportion of coniferous cover. For both BA and stem counts, values above the black line are greater than the mean for the year. Groups with fewer than 3 observations are omitted from the graph.

novel forest structures. Our work builds on prior Landsat studies investigating early spectral responses (Pickell et al., 2016), linking these unique responses to different patterns of recovering forest structure and composition, which will likely persist in future forests (Johnstone et al., 2010). Using Landsat time series, we show it is possible to identify unique spectral responses and group them by longer-term patterns of structural recovery. Our spectral clustering approach used multiple spectral indices

to characterize unique spectral trajectories early on after wildfire. We relate these spectral trajectories to forest structure measures, collected via RPAS lidar, from sites at different stages of structural recovery postfire. Overall, sites at different postfire stages showed typical patterns of early structural forest development, including stand initiation and stem exclusion (Bartels et al., 2016; Oliver & Larson, 1996). However, patterns of structural development varied across spectral clusters.
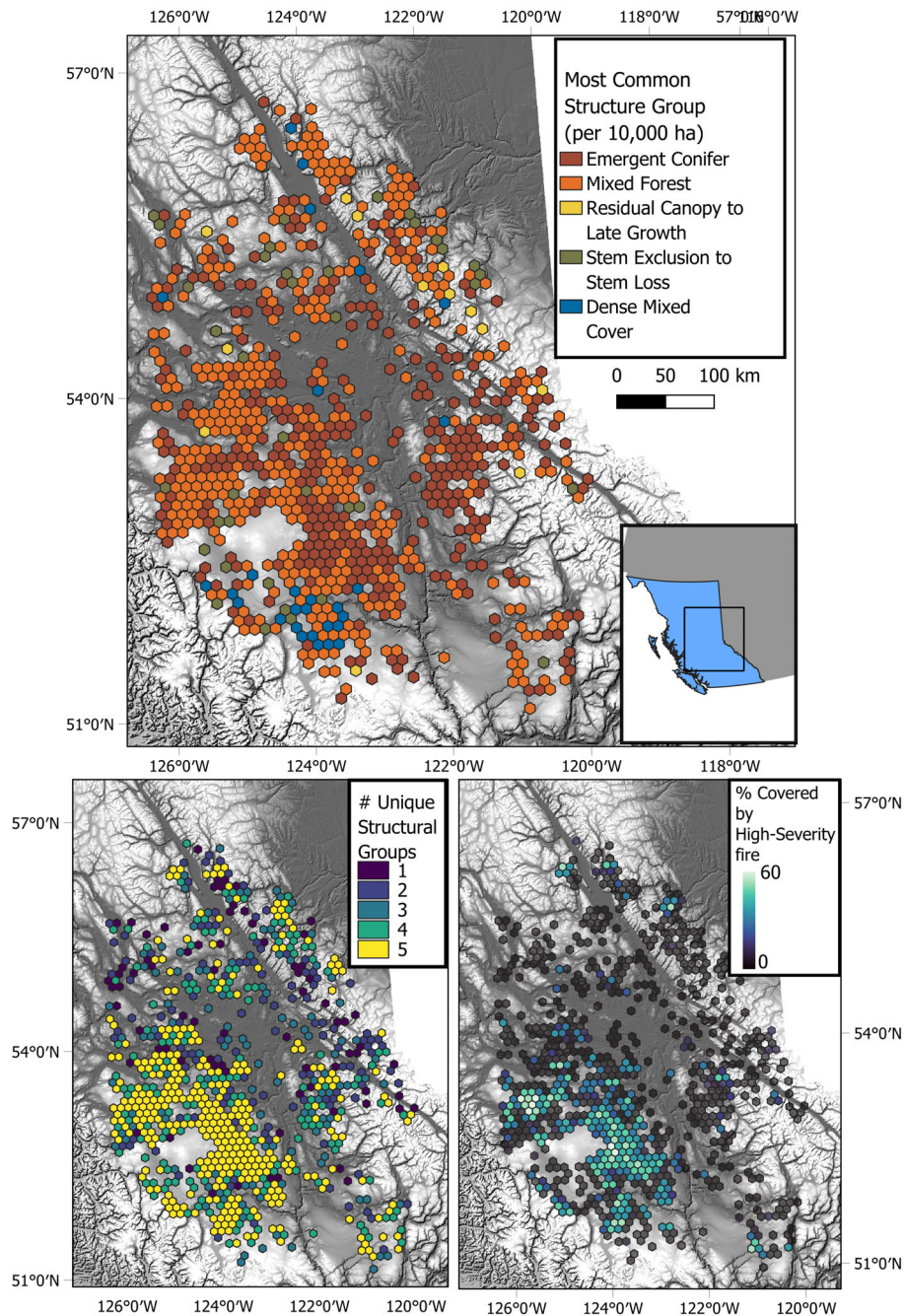
**Figure 7.** (Top) Most common structural groups represented in 10 000 ha hexagons. (Bottom-left) number of distinct structural patterns in each hexagon. (bottom-right) proportion of the hexagon covered by high-severity wildfire. The background for all maps is a hill shade.

Our study highlights two patterns of structural recovery which dominated the majority of the postfire landscape. Patterns included: (1) mixed forest, where the bare ground was gradually infilled with a mix of deciduous and coniferous stems, and (2) emergent conifer, associated with a rapid deciduous response followed by ingrowth of coniferous stems. A minority (20%) of the landscape was covered by other distinctive patterns, including areas with remaining live canopy (residual canopy to late stem growth), strong stem exclusion (stem exclusion to stem loss), or covered by mixed herbaceous and coniferous vegetation (dense mixed cover). For less common patterns, capturing temporal structural growth with space-for-time sampling was difficult.

**(A)**



**(B)**
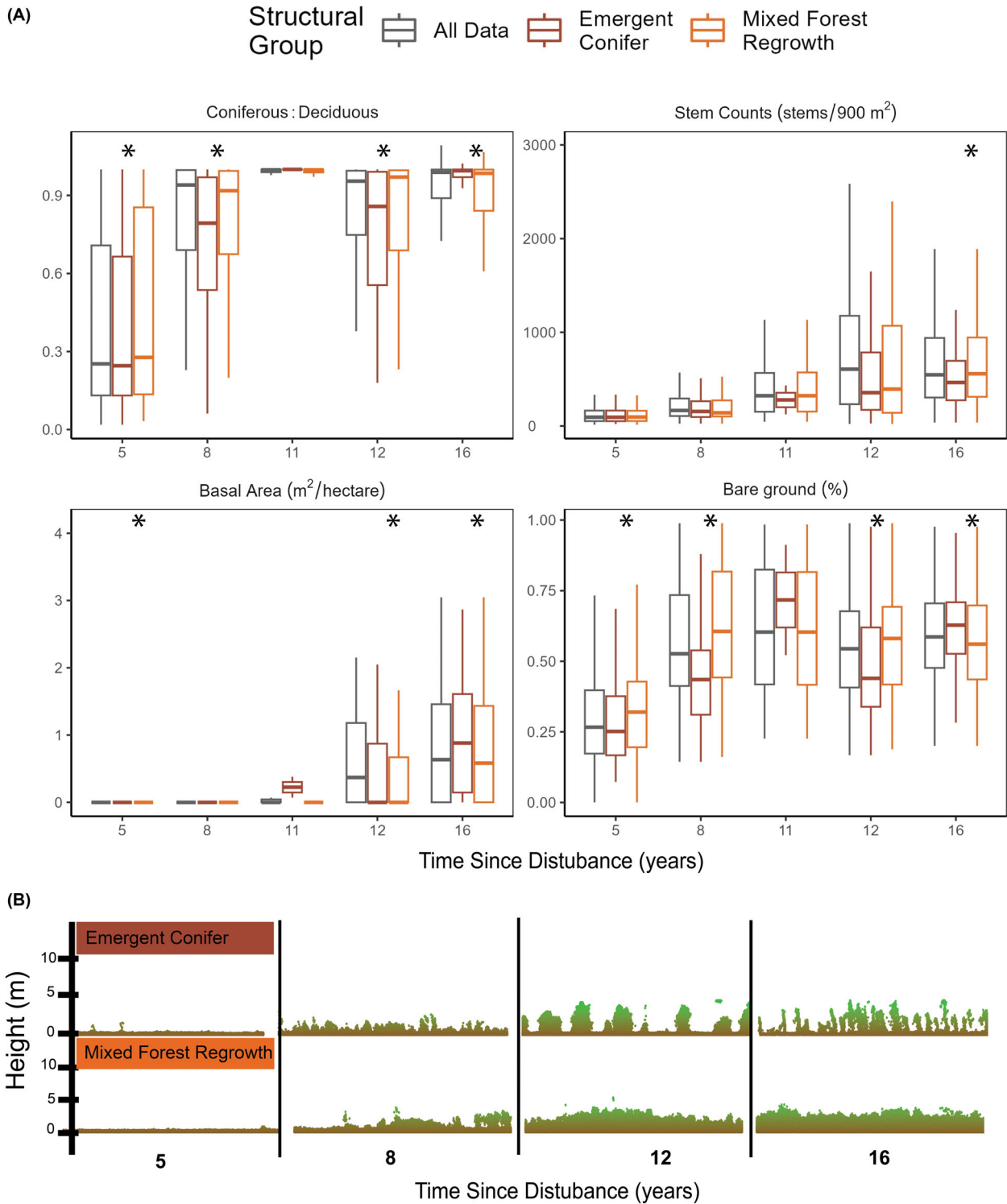


**Figure 8.** (A) Estimates for each structural measure for years after fire. All data (gray) are estimates across all groups. Emergent conifer (red) and mixed forest growth (orange) are subsets for visualization. Asterisks indicate when ANOVA and posthoc Dunn test identify significant (<0.05) differences among the emergent conifer and mixed forest groups (B) Exemplar lidar cross-sections for emergent conifer and mixed forest regrowth groups.

## Multiple spectral indices help differentiate unique spectral dynamics

Multiple indices in spectral clustering were necessary to delineate unique spectral responses. NBR and TCA captured the most variability of spectral responses. We expected NBR and TCA to be influential as these indices capture soil reflectance and vegetation growth in young and dynamic forest types (Cohen et al., 2020; Gómez et al., 2014). Similar to prior research, we found that TCB was the least informative index for clustering (Smith-Tripp et al., 2024). The importance of TCB is likely minimal, 1-18 as TCB saturates rapidly after a disturbance due to ingrowth of deciduous vegetation (Bolton et al., 2018). In our research, NDMI was not informative for cluster development. In general, the use of NDMI for monitoring forests is variable in the literature. Some suggest NDMI is a preferred index (Fornacca et al., 2018; Ochtyra et al., 2020), while others have shown it to be a poor indicator of structure (Cohen et al., 2020; Storey et al., 2016).

The value of multiple spectral indices for structural assessment was further highlighted when clusters were associated with distinct structural groups. Despite the unique spectral responses of clusters 3, 4, 5, and 8, these clusters merged into a single common pattern of mixed forest recovery. Among these spectral clusters, cluster 3 had the highest NBR recovery rate and cluster 5 had the lowest, but other spectral responses were similar, such as the relatively low values of TCW growth. TCW reflectance has a greater sensitivity to stand structure, such as BA; therefore, low values in years 8–16 for this class could be indicative of lower BA growth compared to the emergent conifers group (Viana-Soto et al., 2020).

## Dominant patterns of structural recovery vary in time and space

Different environmental attributes, such as soil moisture, may explain the variable distribution of structural recovery observed across our study region (White et al., 2019). In the study area's drier southwest region, mixed forest regrowth and dense mixed cover were more common than the structural pattern of emergent conifers. Precipitation is widely acknowledged to impact coniferous stem growth (Bright et al., 2019; White et al., 2023; Young et al., 2019); thus, the increased frequency of structural patterns with low coniferous values in the southern regions may be associated with drier conditions. Further, spectral indices themselves probably captured some environmental differences in southern regions. For example, the stem growth to stem loss class was also common in drier southern areas and had particularly low TCW values

(a measure of landscape wetness; Pontone et al., 2024). Differences in precipitation, site aridity, and productivity may also explain the increased heterogeneity in the number of represented structural patterns when a high proportion of the landscape is covered in high-severity fire. Increased representation of structural response patterns may be linked with better representation of site-level differences (e.g., site aridity), which can impact patterns of structural development (Hamilton & Burton, 2023; Talucci et al., 2019). Investigating environmental controls on structural recovery is outside the scope of the current investigation but is possible using our methodology.

## Early spectral dynamics linked with incipient recovery as a tool for land management

Early spectral recovery was indicative of longer-term differences in forest structural development. For example, emergent conifer areas had the highest TCG regrowth of the first 5 years, which was likely influenced by their rapid deciduous ingrowth. The importance of TCG in capturing this deciduous growth has been shown in previous postdisturbance studies (Pickell et al., 2016). Early spectral reflectance also captured the senescence of live canopy in the residual canopy group between years 5 and 8. The residual canopy group had the lowest TCB regrowth values, indicating a steady increase in duff and litter as the live canopy fell to the ground (Banskota et al., 2014).

By combining Landsat time series with RPAS lidar data, we found that distinct early spectral responses were associated with different temporal patterns of structural recovery, including patterns of deciduous growth and stand density. These patterns of structural recovery varied spatially, suggesting that environmental conditions may influence structural development across our study area. Our research supports that there is generally a low risk of coniferous establishment failure in the SBS and SPBS (Clason et al., 2022), but many regions also have a strong proportion of deciduous stems. Although increasing deciduous cover may be undesirable for timber-based management objectives, it may be advantageous for increased resilience to warming climates (Morin et al., 2018) and decreased fire risk (Prichard et al., 2021). In areas with numerous residual live trees, canopy senescence can contribute to deadwood fuel buildup, which increases future fire risk (Prichard et al., 2021), but the remaining canopy can increase the diversity of regenerating tree species (Clason et al., 2022; Meddens et al., 2018) and provide numerous other non-timber values. Balancing the risk associated with postfire fuel build-up, with benefits of increased diversity requires nuanced knowledge

of site dynamics; while our approach does not capture these site dynamics directly, our methodology effectively identifies priority areas for further investigation and more intensive management (Pettorelli et al., 2018).

## Conclusion

Our research leverages the legacy of Landsat alongside the expanding availability of RPAS lidar data to identify patterns of structural recovery. British Columbia's increasingly disturbed area requires monitoring that projects expected shifts in forest structure early on after fire events (Crausbay et al., 2022). By quantifying the relationships between early postdisturbance spectral responses and forest structural attributes at a critical recovery juncture, the methodology presented herein allows forest managers to make strategic decisions that capitalize on shifts in climate and species ranges (Hessburg et al., 2021; Pettorelli et al., 2018).

## Acknowledgments

## References

Anderson, M.J. (2001) A new method for non-parametric multivariate analysis of variance. *Austral Ecology*, **26**, 32–46. Available from: https://doi.org/10.1111/j.1442-9993.2001.01070.pp.x

Baltzer, J.L., Day, N.J., Walker, X.J., Greene, D., Mack, M.C., Alexander, H.D. et al. (2021) Increasing fire and the decline of fire adapted black spruce in the boreal forest. *Proceedings of the National Academy of Sciences of the United States of America*, **118**, e2024872118. Available from: https://doi.org/10.1073/pnas.2024872118

Banskota, A., Kayastha, N., Falkowski, M.J., Wulder, M.A., Froese, R.E. & White, J.C. (2014) Forest monitoring using Landsat time series data: a review. *Canadian Journal of Remote Sensing*, **40**, 362–384. Available from: https://doi.org/10.1080/07038992.2014.987376

Bartels, S.F., Chen, H.Y.H., Wulder, M.A. & White, J.C. (2016) Trends in post-disturbance recovery rates of Canada's forests following wildfire and harvest. *Forest Ecology and Management*, **361**, 194–207. Available from: https://doi.org/10.1016/j.foreco.2015.11.015

BC Ministry of Forests. (2021) 2021 burn severity mapping.

Bolton, D.K., White, J.C., Wulder, M.A., Coops, N.C., Hermosilla, T. & Yuan, X. (2018) Updating stand-level forest inventories using airborne laser scanning and Landsat time series data. *International Journal of Applied Earth Observation and Geoinformation*, **66**, 174–183. Available from: https://doi.org/10.1016/j.jag.2017.11.016

Bright, B.C., Hudak, A.T., Kennedy, R.E., Braaten, J.D. & Khalyani, A.H. (2019) Examining post-fire vegetation recovery with Landsat time series analysis in three western North American forest types. *Fire Ecology*, **15**, 8. Available from: https://doi.org/10.1186/s42408-018-0021-9

Chu, T. & Guo, X. (2014) Remote sensing techniques in monitoring post-fire effects and patterns of Forest recovery in boreal forest regions: a review. *Remote Sensing*, **6**, 470–520. Available from: https://doi.org/10.3390/rs6010470

Clason, A.J., Farnell, I. & Lilles, E.B. (2022) Carbon 5–60 years after fire: planting trees does not compensate for losses in dead Wood Stores. *Frontiers in Forests and Global Change*, **5**, 1–18. Available from: https://doi.org/10.3389/ffgc.2022.868024

Cohen, W.B., Healey, S.P., Yang, Z., Zhu, Z. & Gorelick, N. (2020) Diversity of algorithm and spectral band inputs improves landsat monitoring of forest disturbance. *Remote Sensing*, **12**, 1673. Available from: https://doi.org/10.3390/rs12101673

Cohen, W.B., Maiersperger, T.K., Gower, S.T. & Turner, D.P. (2003) An improved strategy for regression of biophysical variables and Landsat ETM+ data. *Remote Sensing of Environment*, **84**, 561–571. Available from: https://doi.org/10.1016/S0034-4257(02)00173-6

Cohen, W.B., Yang, Z. & Kennedy, R. (2010) Detecting trends in forest disturbance and recovery using yearly Landsat time series: 2. TimeSync — tools for calibration and validation. *Remote Sensing of Environment*, **114**, 2911–2924. Available from: https://doi.org/10.1016/j.rse.2010.07.010

Coops, N.C., Tompalski, P., Goodbody, T.R.H., Queinnec, M., Luther, J.E., Bolton, D.K. et al. (2021) Modelling lidar-derived estimates of forest attributes over space and time: a review of approaches and future trends. *Remote Sensing of Environment*, **260**, 112477. Available from: https://doi.org/10.1016/j.rse.2021.112477

Crausbay, S.D., Sofaer, H.R., Cravens, A.E., Chaffin, B.C., Clifford, K.R., Gross, J.E. et al. (2022) A science agenda to inform natural resource management decisions in an era of ecological transformation. *Bioscience*, **72**, 71–90. Available from: https://doi.org/10.1093/biosci/biab102

Davis, K.T., Robles, M.D., Kemp, K.B., Higuera, P.E., Chapman, T., Metlen, K.L. et al. (2023) Reduced fire severity offers near-term buffer to climate-driven declines in conifer resilience across the western United States. *Proceedings of the National Academy of Sciences of the United States of America*, **120**, e2208120120. Available from: https://doi.org/10.1073/pnas.2208120120

Fornacca, D., Ren, G. & Xiao, W. (2018) Evaluating the best spectral indices for the detection of burn scars at several post-fire dates in a mountainous region of Northwest Yunnan, China. *Remote Sensing*, 10, 1196. Available from: https://doi.org/10.3390/rs10081196

Francini, S. (2021) BAP-GEE.

Frazier, R.J., Coops, N.C., Wulder, M.A., Hermosilla, T. & White, J.C. (2018) Analyzing spatial and temporal variability in short-term rates of post-fire vegetation return from Landsat time series. *Remote Sensing of Environment*, 205, 32–45. Available from: https://doi.org/10.1016/j.rse.2017.11.007

Frolking, S., Palace, M.W., Clark, D.B., Chambers, J.Q., Shugart, H.H., Hurtt, G.C., 2009. Forest disturbance and recovery: a general review in the context of spaceborne remote sensing of impacts on aboveground biomass and canopy structure. *Journal of Geophysical Research-Atmospheres* 114, G00E02. https://doi.org/https://doi.org/10.1029/2008JG000911.

Gómez, C., White, J.C., Wulder, M.A. & Alejandro, P. (2014) Historical forest biomass dynamics modelled with Landsat spectral trajectories. *ISPRS Journal of Photogrammetry and Remote Sensing*, 93, 14–28. Available from: https://doi.org/10.1016/j.isprsjprs.2014.03.008

Guimarães, N., Pádua, L., Marques, P., Silva, N., Peres, E. & Sousa, J.J. (2020) Forestry remote sensing from unmanned aerial vehicles: a review focusing on the data, processing and potentialities. *Remote Sensing*, 12, 1046. Available from: https://doi.org/10.3390/rs12061046

Hamilton, N. & Burton, P. (2023) Wildfire disturbance reveals evidence of ecosystem resilience and precariousness in a forest–grassland mosaic. *Ecosphere*, 14, e4460. Available from: https://doi.org/10.1002/ecs2.4460

Hermosilla, T., Francini, S., Nicolau, A.P., Wulder, M.A., White, J.C., Coops, N.C. et al. (2024) Clouds and image compositing. In: Cardille, J.A., Crowley, M.A., Saah, D. & Clinton, N.E. (Eds.) *Cloud-based remote sensing with Google earth engine: fundamentals and applications*. Cham: Springer International Publishing, pp. 279–302. Available from: https://doi.org/10.1007/978-3-031-26588-4_15

Hermosilla, T., Wulder, M.A., White, J.C., Coops, N.C. & Hobart, G.W. (2018) Disturbance-informed annual land cover classification maps of Canada's forested ecosystems for a 29-year Landsat time series. *Canadian Journal of Remote Sensing*, 44, 67–87. Available from: https://doi.org/10.1080/07038992.2018.1437719

Herve, M. (2023) RVAideMemoire: testing and plotting procedures for biostatistics (manual).

Hessburg, P.F., Prichard, S.J., Hagmann, R.K., Povak, N.A. & Lake, F.K. (2021) Wildfire and climate change adaptation of western North American forests: a case for intentional management. *Ecological Applications*, 31, e02432. Available from: https://doi.org/10.1002/eap.2432

Hoecker, T.J., Parks, S.A., Krosby, M. & Dobrowski, S.Z. (2023) Widespread exposure to altered fire regimes under 2°C warming is projected to transform conifer forests of the Western United States. *Communications Earth & Environment*, 4, 295. Available from: https://doi.org/10.1038/s43247-023-00954-8

Holsinger, L.M., Parks, S.A., Saperstein, L.B., Loehman, R.A., Whitman, E., Barnes, J. et al. (2022) Improved fire severity mapping in the North American boreal forest using a hybrid composite method. *Remote Sensing in Ecology and Conservation*, 8, 222–235. Available from: https://doi.org/10.1002/rse2.238

Johnstone, J.F., Allen, C.D., Franklin, J.F., Frelich, L.E., Harvey, B.J., Higuera, P.E. et al. (2016) Changing disturbance regimes, ecological memory, and forest resilience. *Frontiers in Ecology and the Environment*, 14, 369–378. Available from: https://doi.org/10.1002/fee.1311

Johnstone, J.F., Chapin, F.S., Hollingsworth, T.N., Mack, M.C., Romanovsky, V. & Turetsky, M. (2010) Fire, climate change, and forest resilience in interior AlaskaThis article is one of a selection of papers from the dynamics of change in Alaska's boreal forests: resilience and vulnerability in response to climate warming. *Canadian Journal of Forest Research*, 40, 1302–1312. Available from: https://doi.org/10.1139/X10-061

Johnstone, J.F., Hollingsworth, T.N., Chapin Iii, F.S. & Mack, M.C. (2010) Changes in fire regime break the legacy lock on successional trajectories in Alaskan boreal forest. *Global Change Biology*, 16, 1281–1295. Available from: https://doi.org/10.1111/j.1365-2486.2009.02051.x

Jorgensen, A.G., Alfaro-Sánchez, R., Cumming, S.G., White, A.L., Degré-Timmons, G.É., Day, N. et al. (2023) The influence of postfire recovery and environmental conditions on boreal vegetation. *Ecosphere*, 14, e4605. Available from: https://doi.org/10.1002/ecs2.4605

Kapoor, A., Singhal, A., 2017. A comparative study of K-Means, K-Means++ and Fuzzy C-Means clustering algorithms. In: 2017 3rd International Conference on Computational Intelligence & Communication Technology (CICT). Presented at the 2017 3rd International Conference on Computational Intelligence & Communication Technology (CICT), pp. 1–6. https://doi.org/10.1109/CIACT.2017.7977272.

Kassambara, A. & Mundt, F. (2016) factoextra.

Kemp, K.B., Higuera, P.E. & Morgan, P. (2016) Fire legacies impact conifer regeneration across environmental gradients in the U.S. northern Rockies. *Landscape Ecology*, 31, 619–636. Available from: https://doi.org/10.1007/s10980-015-0268-3

Kennedy, R.E., Yang, Z., Cohen, W.B., Pfaff, E., Braaten, J. & Nelson, P. (2012) Spatial and temporal patterns of forest disturbance and regrowth within the area of the Northwest Forest Plan. *Remote Sensing of Environment*, 122, 117–133. Available from: https://doi.org/10.1016/j.rse.2011.09.024

Kiel, N.G. & Turner, M.G. (2022) Where are the trees? Extent, configuration, and drivers of poor forest recovery 30 years

after the 1988 Yellowstone fires. *Forest Ecology and Management*, **524**, 120536. Available from: https://doi.org/10.1016/j.foreco.2022.120536

Klápště, P., Fogl, M., Barták, V., Gdulová, K., Urban, R. & Moudrý, V. (2020) Sensitivity analysis of parameters and contrasting performance of ground filtering algorithms with UAV photogrammetry-based and LiDAR point clouds. *International Journal of Digital Earth*, **13**, 1672–1694. Available from: https://doi.org/10.1080/17538947.2020.1791267

Klassen, H.A. & Burton, P.J. (2015) Climatic characterization of forest zones across administrative boundaries improves conservation planning. *Applied Vegetation Science*, **18**, 343–356. Available from: https://doi.org/10.1111/avsc.12143

Kodinariya, T. & Makwana, P. (2013) Review on determining of cluster in K-means clustering. *International Journal*, **1**, 90–95.

Meddens, A.J.H., Kolden, C.A., Lutz, J.A., Smith, A.M.S., Cansler, C.A., Abatzoglou, J.T. et al. (2018) Fire refugia: what are they, and why do they matter for global change? *Bioscience*, **68**, 944–954. Available from: https://doi.org/10.1093/biosci/biy103

Meidinger, D.V. & Pojar, J. (1991) *Ecosystems of British Columbia*. Victoria, BC: B.C. Ministry of Forests.

Metsaranta, J.M., Hudson, B., Smyth, C., Fellows, M. & Kurz, W.A. (2023) Future fire risk and the greenhouse gas mitigation potential of forest rehabilitation in British Columbia, Canada. *Forest Ecology and Management*, **529**, 120729. Available from: https://doi.org/10.1016/j.foreco.2022.120729

Morin, X., Fahse, L., Jactel, H., Scherer-Lorenzen, M., García-Valdés, R. & Bugmann, H. (2018) Long-term response of forest productivity to climate change is mostly driven by change in tree species composition. *Scientific Reports*, **8**, 5627. Available from: https://doi.org/10.1038/s41598-018-23763-y

Mouselimis, L. (2023) ClusterR: gaussian mixture models, K-means, mini-batch-kmeans, K-medoids and affinity propagation clustering (manual).

North, M.P., Stevens, J.T., Greene, D.F., Coppoletta, M., Knapp, E.E., Latimer, A.M. et al. (2019) Tamm review: reforestation for resilience in dry western U.S. forests. *Forest Ecology and Management*, **432**, 209–224. Available from: https://doi.org/10.1016/j.foreco.2018.09.007

Ochtyra, A., Marcinkowska-Ochtyra, A. & Raczko, E. (2020) Threshold- and trend-based vegetation change monitoring algorithm based on the inter-annual multi-temporal normalized difference moisture index series: a case study of the Tatra Mountains. *Remote Sensing of Environment*, **249**, 112026. Available from: https://doi.org/10.1016/j.rse.2020.112026

Oksanen, J., Simpson, G.L., Blanchet, F.G., Kindt, R., Legendre, P., Minchin, P.R. et al. (2022) vegan: community ecology package (manual).

Oliver, C.D. & Larson, B. (1996) Forest stand dynamics.

Parisien, M.-A., Barber, Q.E., Bourbonnais, M.L., Daniels, L.D., Flannigan, M.D., Gray, R.W. et al. (2023) Abrupt, climate-induced increase in wildfires in British Columbia since the mid-2000s. *Communications Earth & Environment*, **4**, 309. Available from: https://doi.org/10.1038/s43247-023-00977-1

Pasquarella, V.J., Holden, C.E., Kaufman, L. & Woodcock, C.E. (2016) From imagery to ecology: leveraging time series of all available Landsat observations to map and monitor ecosystem state and dynamics. *Remote Sensing in Ecology and Conservation*, **2**, 152–170. Available from: https://doi.org/10.1002/rse2.24

Pettorelli, N., Schulte to Bühne, H., Tulloch, A., Dubois, G., Macinnis-Ng, C., Queirós, A.M. et al. (2018) Satellite remote sensing of ecosystem functions: opportunities, challenges and way forward. *Remote Sensing in Ecology and Conservation*, **4**, 71–93. Available from: https://doi.org/10.1002/rse2.59

Pickell, P.D., Hermosilla, T., Frazier, R.J., Coops, N.C. & Wulder, M.A. (2016) Forest recovery trends derived from Landsat time series for North American boreal forests. *International Journal of Remote Sensing*, **37**, 138–149. Available from: https://doi.org/10.1080/2150704X.2015.1126375

Pickett, S.T.A. (1989) Space-for-time substitution as an alternative to Long-term studies. In: Likens, G.E. (Ed.) *Long-term studies in ecology: approaches and alternatives*. New York, NY: Springer, pp. 110–135. Available from: https://doi.org/10.1007/978-1-4615-7358-6_5

Pontone, N., Millard, K., Thompson, D.K., Guindon, L. & Beaudoin, A. (2024) A hierarchical, multi-sensor framework for peatland sub-class and vegetation mapping throughout the Canadian boreal forest. *Remote Sensing in Ecology and Conservation*, **10**, 500–516. Available from: https://doi.org/10.1002/rse2.384

Prichard, S.J., Hessburg, P.F., Hagmann, R.K., Povak, N.A., Dobrowski, S.Z., Hurteau, M.D. et al. (2021) Adapting western North American forests to climate change and wildfires: 10 common questions. *Ecological Applications*, **31**, e02433. Available from: https://doi.org/10.1002/eap.2433

Rakochy, P. & Hawkins, C. (2006) Wildlife/danger tree assessment in unharvested stands attacked by mountain pine beetle in the central interior of British Columbia. *Journal of Ecosystems and Management*, **7**, 72–80.

Roussel, J.-R., Auty, D., Coops, N.C., Tompalski, P., Goodbody, T.R.H., Meador, A.S. et al. (2020) lidR: an R package for analysis of airborne laser scanning (ALS) data. *Remote Sensing of Environment*, **251**, 112061. Available from: https://doi.org/10.1016/j.rse.2020.112061

Sanderson, C. & Curtin, R. (2016) Armadillo: a template-based C++ library for linear algebra. *Journal of Open Source*

*Software*, **1**, 26. Available from: https://doi.org/10.21105/joss.00026

Seidl, R. & Turner, M.G. (2022) Post-disturbance reorganization of forest ecosystems in a changing world. *Proceedings of the National Academy of Sciences*, **119**, e2202190119. Available from: https://doi.org/10.1073/pnas.2202190119

Shrestha, M., Broadbent, E.N. & Vogel, J.G. (2021) Using GatorEye UAV-borne LiDAR to quantify the spatial and temporal effects of a prescribed fire on understory height and biomass in a pine savanna. *Forests*, **12**, 38. Available from: https://doi.org/10.3390/f12010038

Smith-Tripp, S.M., Coops, N.C., Mulverhill, C., White, J.C. & Axelson, J. (2024) Landsat assessment of variable spectral recovery linked to post-fire forest structure in dry sub-boreal forests. *ISPRS Journal of Photogrammetry and Remote Sensing*, **208**, 121–135. Available from: https://doi.org/10.1016/j.isprsjprs.2024.01.008

Storey, E.A., Stow, D.A. & O'Leary, J.F. (2016) Assessing postfire recovery of chamise chaparral using multi-temporal spectral vegetation index trajectories derived from Landsat imagery. *Remote Sensing of Environment*, **183**, 53–64. Available from: https://doi.org/10.1016/j.rse.2016.05.018

Talucci, A.C., Lertzman, K.P. & Krawchuk, M.A. (2019) Drivers of lodgepole pine recruitment across a gradient of bark beetle outbreak and wildfire in British Columbia. *Forest Ecology and Management*, **451**, 117500. Available from: https://doi.org/10.1016/j.foreco.2019.117500

Viana-Soto, A., Aguado, I., Salas, J. & García, M. (2020) Identifying post-fire recovery trajectories and driving factors using Landsat time series in fire-prone Mediterranean pine forests. *Remote Sensing*, **12**, 1499. Available from: https://doi.org/10.3390/rs12091499

White, H.J., Gaul, W., Sadykova, D., León-Sánchez, L., Caplat, P., Emmerson, M.C. et al. (2020) Quantifying large-scale ecosystem stability with remote sensing data. *Remote Sensing in Ecology and Conservation*, **6**, 354–365. Available from: https://doi.org/10.1002/rse2.148

White, J.C. (2024) Characterizing forest recovery following stand-replacing disturbances in boreal forests: contributions of optical time series and airborne laser scanning data. *Silva Fennica*, **58**, 23076.

White, J.C., Hermosilla, T. & Wulder, M.A. (2023) Pre-fire measures of boreal forest structure and composition inform interpretation of post-fire spectral recovery rates. *Forest Ecology and Management*, **537**, 120948. Available from: https://doi.org/10.1016/j.foreco.2023.120948

White, J.C., Hermosilla, T., Wulder, M.A. & Coops, N.C. (2022) Mapping, validating, and interpreting spatio-temporal trends in post-disturbance forest recovery. *Remote Sensing of Environment*, **271**, 112904. Available from: https://doi.org/10.1016/j.rse.2022.112904

White, J.C., Saarinen, N., Wulder, M.A., Kankare, V., Hermosilla, T., Coops, N.C. et al. (2019) Assessing spectral measures of post-harvest forest recovery with field plot data. *International Journal of Applied Earth Observation and Geoinformation*, **80**, 102–114. Available from: https://doi.org/10.1016/j.jag.2019.04.010

White, J.C., Wulder, M.A., Hobart, G.W., Luther, J.E., Hermosilla, T., Griffiths, P. et al. (2014) Pixel-based image compositing for large-area dense time series applications and science. *Canadian Journal of Remote Sensing*, **40**, 192–212. Available from: https://doi.org/10.1080/07038992.2014.945827

Wulder, M.A., Coops, N.C., Hudak, A.T., Morsdorf, F., Nelson, R., Newnham, G. et al. (2013) Status and prospects for LiDAR remote sensing of forested ecosystems. *Canadian Journal of Remote Sensing*, **39**, S1–S5. Available from: https://doi.org/10.5589/m13-051

Ye, S., Rogan, J., Zhu, Z., Hawbaker, T.J., Hart, S.J., Andrus, R.A. et al. (2021) Detecting subtle change from dense Landsat time series: case studies of mountain pine beetle and spruce beetle disturbance. *Remote Sensing of Environment*, **263**, 112560. Available from: https://doi.org/10.1016/j.rse.2021.112560

Young, D.J.N., Werner, C.M., Welch, K.R., Young, T.P., Safford, H.D. & Latimer, A.M. (2019) Post-fire forest regeneration shows limited climate tracking and potential for drought-induced type conversion. *Ecology*, **100**, e02571. Available from: https://doi.org/10.1002/ecy.2571

## Supporting Information

Additional supporting information may be found online in the Supporting Information section at the end of the article.

**Table S1.** Metrics of linear modeling from field plots and RPAS lidar metrics. As linear models included field data that was zero-skewed (BA and stem counts) or proportional we applied different model families, which are noted in the table. For a complete description of ABA modeling see Smith-Tripp et al. (2024).

**Figure S1.** Model graphs comparing field measurements (measured) to model predictions (predicted) built from RPAS lidar. The black line shows the 1:1 line.

**Figure S2.** Average values of each spectral metric input in Kmeans ++ clustering for the eight identified spectral trajectories.

**Table S2.** Results of MANOVA applied to unique spectral clusters to identify structural patterns of recovery. Permutations = 999

**Figure S3.** Post-hoc significance values for analysis of dissimilarities for each cross comparison of clusters. Colors rank similar spectral clusters. We collapsed clusters were post hoc p-values > 0.1.

**Table S3.** Average structural estimate for each structural group for each year after wildfire ($\pm$ standard error of

the mean). The number of observations is the number of $30 \times 30$ m pixels with RPAS lidar data.

**Table S4.** Post-hoc dunn-tests for nested anova comparing emergent conifer and mixed forest structural patterns.

We highlight these groups as they have data across all years. $P$ values are adjusted via the holm method. Years were the structural estimates for each group are different are starred.